Geophysical Journal International

Geophys. J. Int. (2010) **181,** 935–950 doi: 10.1111/j.1365-246X.2010.04540.x

Sequentially ordered single-frequency 2-D acoustic waveform inversion in the Laplace–Fourier domain

Changsoo Shin,[1] Nam-Hyung Koo,[2] Young Ho Cha[1,*] and Keun-Pil Park[2]

[1]*Department of Energy Resources Engineering, Seoul National University,* 599 *Gwanak-ro, Gwanak-gu, Seoul* 151-742, *Korea*
[2]*Petroleum and Marine Research Division, Korea Institute of Geoscience and Mineral Resources,* 92 *Gwahang-no, Yuseong-gu, Daejeon,* 305-350, *Korea.*
E-mail: nhkoo@kigam.re.kr

Accepted 2010 January 25. Received 2009 November 29; in original form 2009 March 13

SUMMARY

In the conventional frequency-domain waveform inversion, either multifrequency simultaneous inversion or sequential single-frequency inversion has been implemented. However, most conventional frequency-domain waveform inversion methods fail to recover background velocity when low-frequency information is missing. Recently, new waveform inversion techniques in the Laplace and Laplace–Fourier domain have been proposed to recover background velocity structure from data with insufficient low-frequency information. In such techniques, however, all frequencies are inverted simultaneously, and this requires large computational resources and long computation times.

In this paper, we propose a sequentially ordered single-frequency 2-D acoustic waveform inversion using the logarithmic objective function in the Laplace–Fourier domain. Our algorithm sequentially inverts single-frequency data in the Laplace–Fourier domain, thus reducing computational resources. Unlike most conventional waveform inversion methods requiring an initial velocity model close to the true model, we propose a one-step waveform inversion method in seeking to find a final velocity structure from the simple initial model through a hybrid combination of the Laplace domain inversion and the Fourier domain inversion.

We adopt and evaluate the multiloop algorithm by modifying the double-loop algorithm commonly used in the conventional frequency-domain waveform inversion. Using the multiloop algorithm repeating loop over frequencies, the quality of the inversion results can be improved and the decision problem of the number of iterations for each frequency can be overcome effectively. Because the sequential order of the Laplace–Fourier frequencies in a 2-D plane should be assigned for inverting Laplace–Fourier frequency data consecutively, we present three different sequential orders of Laplace–Fourier frequencies while considering the multiscale and layer-stripping approach, and we compare the inversion results from the numerical experiments.

We applied the sequentially ordered single-frequency 2-D acoustic waveform inversion in the full Laplace–Fourier domain to the synthetic seismic data produced from complex structure model and field data. A realistic model could be recovered in an efficient and robust manner, even using the two-layer homogeneous velocity model as an initial model. The inverted velocity model from the field data was validated by examining the migrated image from the pre-stack depth migration and the flattening of the common-image gathers or by comparing the synthetic shot gather with the real shot gather. The proposed one-step waveform inversion algorithm can be easily extended to the sequential inversion of 3-D acoustic or elastic data in the full Laplace–Fourier domain.

Key words: Inverse theory; Seismic tomography; Computational seismology; Acoustic properties.

INTRODUCTION

The non-linear waveform inversion seeks to derive subsurface physical properties such as velocity, density, Q values, by iteratively minimizing the differences between observed data and synthetic

*Now at: ExxonMobil Upstream Research Company, 3120 Buffalo Speedway, Houston, TX 77046, USA.

data, usually in a least squares sense. Since Lailly (1983) and Tarantola (1984) recognized that the model could be updated through an efficient calculation of the gradient by back-propagating the residuals, a considerable amount of research on the non-linear waveform inversion has been carried out (Tarantola 1986; Mora 1987; Pratt & Worthington 1990; Bunks *et al.* 1995; Pratt *et al.* 1998; Shin & Min 2006). Waveform inversion can be implemented either in the time domain or in the frequency domain. Time-domain waveform inversion has rarely been applied to field data due to the large computation resources and long time required for multiple sources and receivers, and difficulty of the unknown source wavelet estimation (Mora 1987; Shipp & Singh 2002; Sheen *et al.* 2006). In contrast, 2-D frequency-domain waveform inversion might be more practical because multiple shot acquisition can be simulated efficiently and the unknown source wavelet can be estimated simultaneously during waveform inversion (Marfurt 1984; Pratt 1999; Shin & Min 2006).

In frequency-domain waveform inversion, three inversion approaches have been tried: a multifrequency simultaneous inversion (Lee & Kim 2003; Shin & Min 2006; Hu *et al.* 2007), a sequential single-frequency inversion (Yokota & Matsushima 2004; Sirgue & Pratt 2004; Operto *et al.* 2006; Ben-Hadj-Ali *et al.* 2008) and a combination of both approaches (Pratt 1999; Brenders & Pratt 2007; Bleibinhaus *et al.* 2008; Jaiswal *et al.* 2008). In the multifrequency simultaneous inversion, just as all time samples are inverted simultaneously in the time domain, all frequencies are inverted simultaneously (Lee & Kim 2003; Shin & Min 2006; Hu *et al.* 2007). Note that not all of the discrete frequencies need to be inverted, and that a coarse frequency-sampling interval can be used in the frequency-domain inversion. However, the simultaneous inversion process requires large computational resources, such as a high-performance parallel or a massively parallel system, to handle the large number of shots or frequencies effectively. In addition, to balance the contributions from the different frequency components, proper scaling of the steepest-descent direction or data-weighting scheme should be applied (Hu *et al.* 2007; Jang *et al.* 2009). Based on the facts that (1) a finite region in the wavenumber domain can be obtained from a single-frequency component, depending on the acquisition geometry and (2) the inherent nonlinearity of the waveform inversion problem can be mitigated when the low-frequency data are inverted initially because the low-frequency data are less nonlinear with the model than high-frequency data, a sequential single-frequency inversion has been attempted that successively inverts from low- to high-frequency data (Wu & Toksöz 1987; Yokota & Matsushima 2004; Sirgue & Pratt 2004; Operto *et al.* 2006; Ben-Hadj-Ali *et al.* 2008). Moreover, a sequential single-frequency inversion requires less computational resources than the multifrequency simultaneous inversion and a proper scaling or data-weighting problem is not an issue. In an approach that combines the multifrequency simultaneous inversion and the sequentially ordered single-frequency inversion, contiguous or overlapping groups of increasingly higher frequencies are inverted sequentially, and all frequencies in each group are inverted simultaneously (Pratt 1999; Brenders & Pratt 2007; Bleibinhaus *et al.* 2008; Jaiswal *et al.* 2008). From the viewpoint of computational resources, a sequentially ordered single-frequency inversion is most efficient.

When we use a local descent approach and the initial model is far from the true model, the gradient will converge, not to the global minimum, but to the nearest local minimum. Especially in the case when low-frequency information is missing in the seismic data, we cannot recover low wavenumbers or long wavelengths of the background velocity. Therefore, previous waveform inversion researches have been carried out as a two-step process: (1) estimation of the macromodel sufficiently close enough to the true model and (2) addition of short-wavelength characteristics. Most commonly, a traveltime tomography result from the first process or a smoothed version of the true velocity model is used as a starting model for the waveform inversion as a second process (Sirgue & Pratt 2004; Operto *et al.* 2006; Brenders & Pratt 2007; Ben-Hadj-Ali *et al.* 2008; Bleibinhaus *et al.* 2008; Jaiswal *et al.* 2008). Recently, a novel waveform inversion technique, waveform inversion in the Laplace and Laplace–Fourier domain, was proposed to recover a background velocity model even from data suffering from a lack of low-frequency information (Shin & Cha 2008, 2009). Waveform inversion in the Laplace and Laplace–Fourier domain tries to invert Laplace-transformed wavefields, which are zero- or low-frequency components of damped wavefields using several damping constants. The objective function in the Laplace domain is smoother and has fewer local minima than the conventional frequency-domain waveform inversion (Shin & Ha 2008). Although this does not guarantee the convergence to a global minimum, many numerical experiments of the Laplace-domain waveform inversion have produced a smooth velocity model in a robust manner, even from simple starting models such as the two-layer velocity model or the linearly increasing velocity model (Shin & Cha 2008, 2009; Shin & Ha 2008). However, the Laplace- and Laplace–Fourier domain waveform inversions have been implemented as a simultaneous inversion for several Laplace damping constants and frequencies, thus requiring large computational resources. In addition, the final velocity model was still produced from the two-step process (Shin & Cha 2009).

In this paper, we propose a one-step waveform inversion algorithm, a sequentially ordered single-frequency 2-D acoustic waveform inversion using the logarithmic objective function in the Laplace–Fourier domain. Our algorithm sequentially inverts single-frequency data in the Laplace–Fourier domain and seeks to find a final velocity structure from a simple initial model through a hybrid combination of both the Laplace domain inversion and the Fourier domain inversion. We first review the wavefields in the Laplace–Fourier domain and single-frequency logarithmic waveform inverse theory. Then, we demonstrate that the multiloop sequential inversion can improve the quality of the inversion results and effectively overcome the decision problem of the number of iterations for each frequency. We present the inversion results for three different sequential orders of Laplace–Fourier frequencies. Finally, we demonstrate our algorithm by applying it to synthetic seismic data produced from the complex structure model and the field data.

THEORY

Review of the wavefields in the Laplace–Fourier domain

A time-domain wavefield can be decomposed as a series of sinusoidal waves by the Fourier transform. The Fourier transform is given by the expression

$$\widetilde{u}(\omega) = \int_0^\infty u(t)\mathrm{e}^{-i\omega t}\,dt, \tag{1}$$

where ω is an angular frequency, $u(t)$ is a time-domain wavefield and i is $\sqrt{-1}$.

Similarly, a time-domain wavefield can be transformed to a Laplace-transformed wavefield by the Laplace Transform, which

is given by the expression

$$\widetilde{u}(\sigma) = \int_0^\infty u(t)\mathrm{e}^{-\sigma t}\,dt, \tag{2}$$

where σ is the positive Laplace damping constant or Laplace frequency.

If we introduce a complex-valued angular frequency in eq. (1) or a complex-valued damping factor in eq. (2), a time-domain wavefield can be decomposed as a series of damped sinusoidal waves by the Laplace–Fourier Transform, which is given by the expression

$$\widetilde{u}(s) = \widetilde{u}(\sigma,\omega) = \int_0^\infty u(t)\mathrm{e}^{-\sigma t}\mathrm{e}^{-i\omega t}\,dt. \tag{3}$$

We will refer to a complex-valued damping factor as a Laplace–Fourier frequency to differentiate it from frequencies used in conventional frequency-domain waveform inversions. Observed data in the time domain can be transformed to those in the Laplace–Fourier domain by the numerical integration method (Shin & Cha 2008).

To understand the conventional frequency-domain wavefield, the Laplace-domain wavefield and the Laplace–Fourier domain wavefield, we transformed a synthetic seismogram of the BP model (Billette & Brandsberg-Dahl 2005) shown in Fig. 1(a) to each domain. Fig. 1(b) shows the Laplace–Fourier wavefield domain. The horizontal axis is the temporal frequency axis and the vertical axis is the Laplace damping constant or Laplace frequency axis. Figs 1(c) and (d) show the amplitude and phase spectra of the 1, 2 and 5 Hz components for the Laplace damping constant 0.01, which are used for the conventional frequency-domain wavefield. The amplitude and phase spectra are highly variable with the offset. Figs 1(e) and (f) show the amplitude and phase spectra of the 0.01, 1, 2 and 5 Hz components for the Laplace damping constant 3. We note that the amplitude and phase spectra for the larger damping constant (Figs 1e and f) are obviously smoother than the smaller damping constant (Figs 1c and 1d). The amplitude spectra decrease exponentially with the offset, and the smaller variations are added as the frequency increases. Figs 1(g) and (h) show the amplitude and phase spectra of 0.01 Hz for different damping constants, which are used for the Laplace-domain waveform inversion. Note that the amplitude spectra decrease exponentially with the offset and that they decrease more rapidly as the Laplace damping constant becomes larger. The phase spectrum is about zero because the frequency is almost zero. Considering these characteristics of Laplace-transformed wavefields with amplitudes that are too small and the advantage of the natural separation of amplitude and phase spectra of the logarithmic waveform inversion, the logarithmic objective function is suitable for waveform inversion (Shin & Min 2006; Shin & Cha 2008). Figs 1(i) and (j) show the amplitude and phase spectra of 2.0 Hz for different damping constants. The behaviour of the amplitude spectra of 2 Hz is similar to that of 0.01 Hz, but small variations are added. The phase spectrum becomes smoother as the damping constant becomes larger. Note that the variation of the phase spectrum for the large damping constant is related to the first arrival times.

Forward modelling in the Laplace–Fourier domain

The discretized equation for the acoustic wave equation using the finite-element approach can be written as

$$\mathbf{M}\ddot{\mathbf{u}}(t) + \mathbf{C}\dot{\mathbf{u}}(t) + \mathbf{K}\mathbf{u}(t) = \mathbf{f}(t), \tag{4}$$

where $\mathbf{M}$ is the mass matrix, $\mathbf{C}$ is the damping matrix,$\mathbf{K}$ is the stiffness matrix, $\mathbf{u}(t)$ is a discretized wavefield in the time domain and $\mathbf{f}(t)$is a discretized source vector (Marfurt 1984).

In the Laplace–Fourier domain, eq. (4) can be expressed as

$$s^2\mathbf{M}\tilde{\mathbf{u}}(s) + s\mathbf{C}\tilde{\mathbf{u}}(s) + \mathbf{K}\tilde{\mathbf{u}}(s) = \tilde{\mathbf{f}}(s), \tag{5}$$

where

$$\tilde{\mathbf{u}}(s) = \int_0^\infty \mathbf{u}(t)\mathrm{e}^{-st}\,dt, \tag{6}$$

$$\tilde{\mathbf{f}}(s) = \int_0^\infty \mathbf{f}(t)\mathrm{e}^{-st}\,dt \tag{7}$$

and s is a complex-valued damping factor or Laplace–Fourier frequency, $\sigma + i\omega$ and σ is a positive Laplace damping factor.

For simplicity, eq. (5) can be rewritten as

$$\mathbf{S}\tilde{\mathbf{u}}(s) = \tilde{\mathbf{f}}(s), \tag{8}$$

where the complex impedance matrix, $\mathbf{S}$, is given by $\mathbf{K}+s\mathbf{C}+s^2\mathbf{M}$. The complex impedance matrix depends on the model parameters. If we consider the constant-density, isotropic, 2-D acoustic wave propagation, the model parameter will be the 2-D velocity.

In the same manner as the conventional forward modelling in the frequency domain, the forward modelled data in the Laplace–Fourier domain can be computed by an LU factorization of the complex impedance matrix and forward and backward substitutions for multiple source vectors.

Single-frequency logarithmic waveform inversion theory

In the single-frequency Laplace–Fourier domain waveform inversion algorithm, the residual at the jth receiver for the ith source for a single complex-valued frequency or single complex-valued Laplace damping factor can be defined as the logarithmic ratio between synthetic data in a given model, $\widetilde{u}_{ij}$, and observed data, $\widetilde{d}_{ij}$, in the Laplace–Fourier domain (Shin & Min 2006). Thus,

$$\delta r_{ij} = \ln(\widetilde{u}_{ij}) - \ln(\widetilde{d}_{ij}) = \ln\left(\frac{\widetilde{u}_{ij}}{\widetilde{d}_{ij}}\right). \tag{9}$$

We are trying to find a solution by minimizing, in a least squares sense, the objective function defined as

$$E(\mathbf{p}) = \frac{1}{2}\sum_{i=1}^{n_\mathrm{s}}\sum_{j=1}^{n_\mathrm{r}} \delta r_{ij}\delta r_{ij}^*, \tag{10}$$

where the superscript $*$ represents complex conjugation, and n_s and n_r are the number of sources and receivers, respectively.

To iteratively update model parameters using the steepest descent method, we calculate the steepest descent direction by taking partial derivatives of eq. (10) with respect to the model parameter, p_k. Thus,

$$\nabla_k E = \frac{\partial E}{\partial p_k} = \sum_{i=1}^{n_s} (\mathbf{v}_k)^T \left(\mathbf{S}^{-1}\right)^T \mathbf{r}_i, \tag{11}$$

where

$$\mathbf{v}_k = -\frac{\partial \mathbf{S}}{\partial p_k}\widetilde{\mathbf{u}}_i, \tag{12}$$

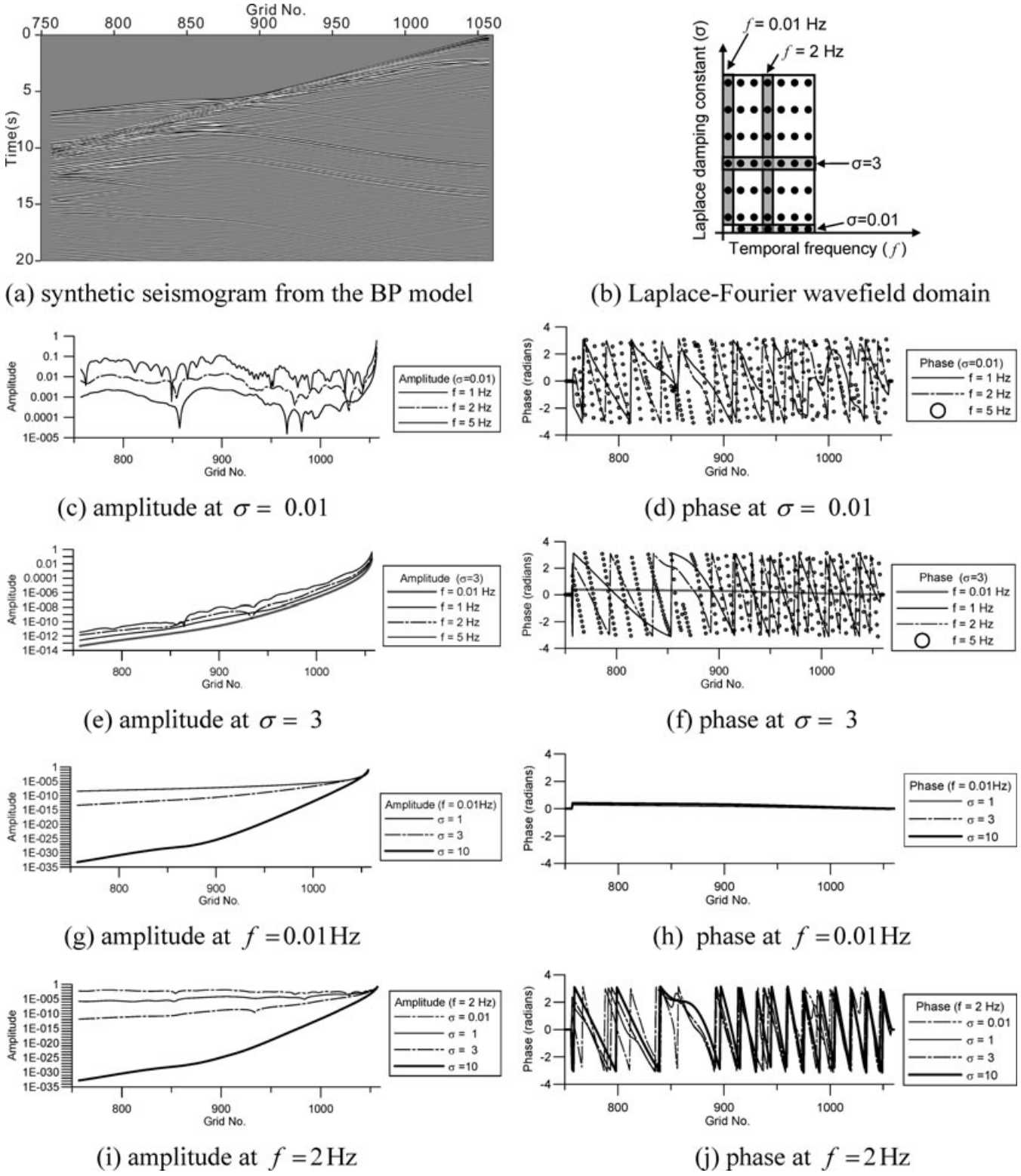

Figure 1. The Laplace–Fourier transformed wavefields for (a) the synthetic shot gather of the BP model. (b) The Laplace–Fourier wavefield domain. Amplitude (c, e, g and i) and phase (d, f, h and j) spectra of the Laplace–Fourier transform with different Laplace–Fourier frequencies: (c,d) for $\sigma = 0.01$, (e,f) for $\sigma = 3$, (g,h) for $f = 0.01$Hz and (i,j) for $f = 2$Hz; (c) and (d) are used for conventional frequency-domain waveform inversion; (g) and (h) are used for Laplace domain waveform inversion.

$$\mathbf{r}_i = \begin{Bmatrix} \ln\left(\widetilde{u}_{i1}/\widetilde{d}_{i1}\right)^* / \widetilde{u}_{i1} \\ \ln\left(\widetilde{u}_{i2}/\widetilde{d}_{i2}\right)^* / \widetilde{u}_{i2} \\ \vdots \\ \ln\left(\widetilde{u}_{in_r}/\widetilde{d}_{in_r}\right)^* / \widetilde{u}_{in_r} \\ 0 \\ \vdots \\ 0 \end{Bmatrix}. \tag{13}$$

In eq. (11), T represents the matrix or vector transpose and $\mathbf{v}_k$ is the virtual source, which is the secondary source for computing the partial derivative of the wavefield (Pratt *et al.* 1998; Shin *et al.* 2001; Shin & Min 2006). The steepest descent direction can be obtained by back-propagating the residuals and computing the scalar product of the back-propagated wavefield and virtual sources (Pratt *et al.* 1998).

By following the suggestion of Shin *et al.* (2001), the steepest descent direction is scaled by the diagonal of the pseudo-Hessian matrix, which is computed by the virtual source vectors. The normalized model update at each complex-valued frequency at the lth iteration can be expressed as

$$\Delta p_k^l = NRM \left\{ \frac{\sum_{i=1}^{n_s} (\mathbf{v}_k)^T \mathbf{S}^{-1} \mathbf{r}_i}{\sum_{i=1}^{n_s} (\mathbf{v}_k^*)^T \mathbf{v}_k + \lambda} \right\}, \tag{14}$$

where λ is a Lagrangian multiplier to avoid a singularity problem, and *NRM* is the normalizing operation using the maximum absolute value of the scaled steepest descent vector. Finally, by multiplying the normalized model update by the step length α, the model parameter at each iteration is updated by

$$\begin{aligned} p_k^{l+1} &= p_k^l - \alpha \Delta p_k^l \\ &= p_k^l - \alpha NRM \left\{ \frac{\sum_{i=1}^{n_s} (\mathbf{v}_k)^T \mathbf{S}^{-1} \mathbf{r}_i}{\sum_{i=1}^{n_s} (\mathbf{v}_k^*)^T \mathbf{v}_k + \lambda} \right\}. \end{aligned} \tag{15}$$

In the iterative waveform inversion, to compute forward-modelled data accurately, the source wavelet should be estimated at each step of iteration. In this paper, the source wavelet estimation was carried out using the full Newton method proposed by Shin *et al.* (2007).

MULTILOOP IMPLEMENTATION OF THE SEQUENTIALLY ORDERED SINGLE-FREQUENCY WAVEFORM INVERSION

Conventional frequency-domain waveform inversion

The sequentially ordered single-frequency waveform inversion in the conventional frequency domain has been implemented mostly as a double-loop algorithm (Yokota & Matsushima 2004). In a single-frequency loop, a specific number of iterations are performed per frequency. After each single-frequency loop, the frequency is successively changed for the next loop. If the number of iterations per frequency is n_{iter} and the number of frequencies is n_f, we will obtain the final inversion result after $n_{iter} \times n_f$ iterations. However, it is difficult to determine how many iterations we must perform at each frequency. Usually, we judge the stopping point from the monotonously decreasing features of the misfit function for each frequency. Sometimes we perform several runs of waveform inversion using different numbers of iterations per frequency. We then compare the final models from the highest frequency or the synthetic data with the field data, and choose the models that are reasonable.

In this paper, we adopt the multiloop implementation for the sequentially ordered single-frequency logarithmic waveform inversion (Fig. 2). The inner loop, as a single-frequency loop, is over iterations per frequency. The middle loop is over frequencies. The double-loop in the conventional waveform inversion consists of these two loops, and the number of total iterations will be $n_{iter} \times n_f$. The outer loop indicates the iterations of the middle loop. Therefore, after finishing the middle loop over the frequencies once, we will go back to the first frequency and restart the inversion using the inverted velocity model at the last frequency as a starting model. If we iterate the middle loop n_{loop} times, we will get the final inversion result after $n_{iter} \times n_f \times n_{loop}$ iterations. We will show the numerical examples of the multiloop algorithm of the conventional frequency-domain waveform inversion in the following chapter.

Applying the multiloop implementation to the waveform inversion in the Laplace and Laplace–Fourier domains

The multiloop implementation can be applied to the sequentially ordered single-frequency inversion in the Laplace and Laplace–Fourier domain waveform inversion. The main differences are the composition of the frequencies used, the corresponding wavefields and the sequential order (Fig. 3). First, the frequencies used in the conventional frequency-domain waveform inversion are normally complex-valued frequencies with small damping constants. Next, the frequencies used in the Laplace-domain waveform inversion are complex-valued damping constants or frequencies with zero or very small frequencies, but with several damping constants (Shin & Cha 2008; Fig. 3a). Finally, the frequencies used in the Laplace–Fourier domain waveform inversion are complex-valued frequencies with several low frequencies and several damping constants (Shin & Cha 2009; Fig. 3a).

The waveform inversion in the Laplace domain can be regarded as single-frequency, zero-frequency or dc inversion, but with several different damping constants. The Laplace damping constant controls the depth window of the inverted area. When the damping constant is large, shallow parts of the model are inverted. On the other hand, when the damping constant is small, shallow and deep parts of the model are inverted. When we try to sequentially invert the wavefields with different damping constants, it seems reasonable to sequentially invert large to small damping constants. However, although we do not show the results here, two sequential inversions from large to small damping constants, or from small to large damping constants, produce similar results because we adopt the multiloop implementation.

The waveform inversion in the Laplace–Fourier domain can be regarded as a waveform inversion of multiple frequencies and multiple damping constants. The wavefield domain, then, is a 2-D plane and we have to assign a sequential order of complex-valued frequencies in the 2-D plane to perform the sequential inversion. Following the conventional multiscale inversion approach, we can perform a series of single-frequency inversions from low to high frequencies. However, each single-frequency inversion can be performed as two kinds of a series of single Laplace damping constant inversions: (1) a large to small damping constant or (2) a small to large damping constant. We can also perform a series of multiscale inversions in a layer-stripping manner. We sequentially invert low to high

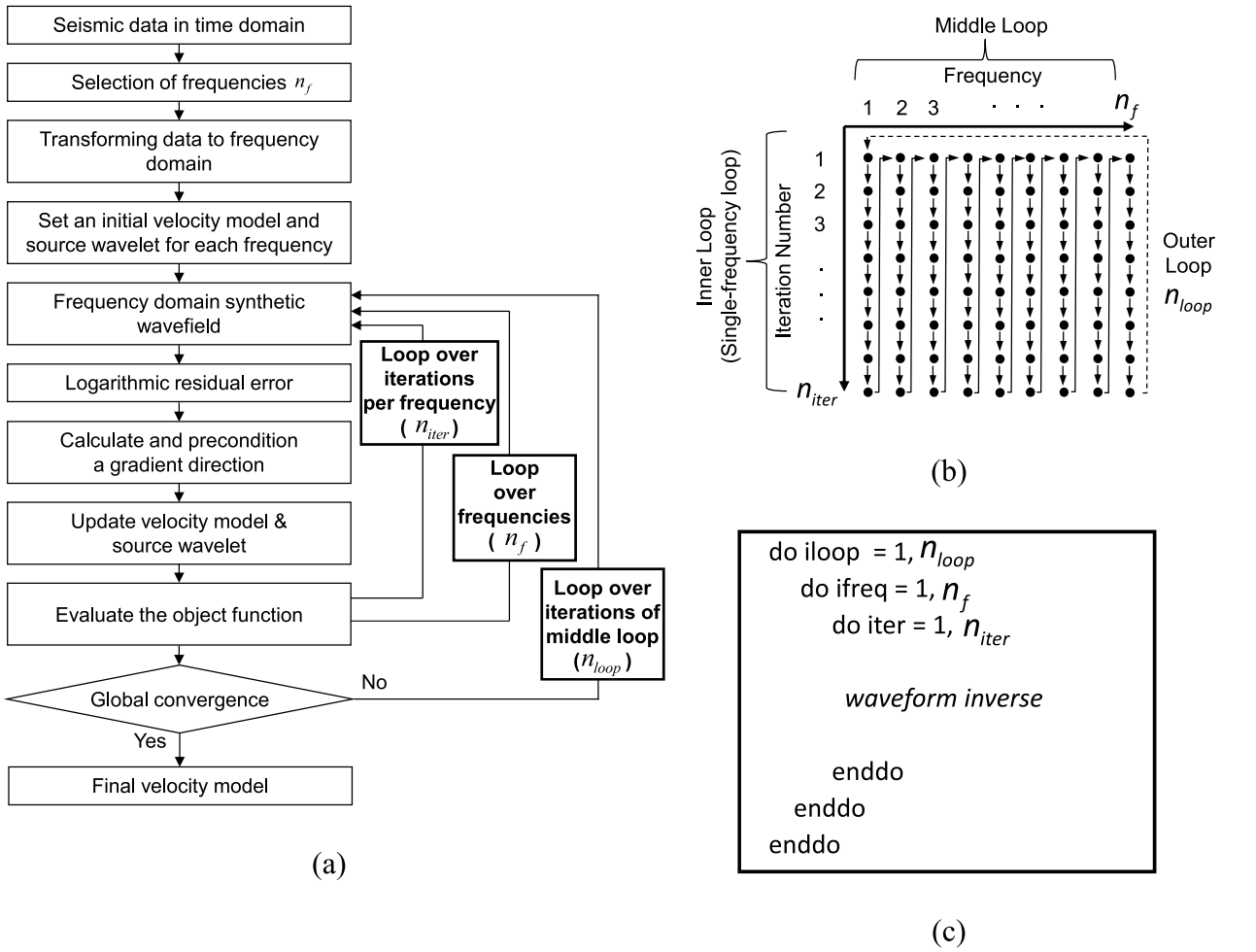

Figure 2. A flowchart (a), a diagram (b) and a simple program structure (c) of the multiloop algorithm of the sequentially ordered single-frequency logarithmic waveform inversion. The inner loop as a single-frequency loop is over iterations per frequency. The middle loop is over frequencies. The outer loop indicates the iterations of the middle loop. In the multiloop algorithm, the inverted model at the last frequency of the previous loop is used as a starting model for the waveform inversion at the first frequency of the next loop.

frequencies at the largest damping constant and iterate sequential inversions at successively lower damping constants. Three sequential orders that we can suppose are shown in Figs 3(b), (c) and (d).

One-step sequential waveform inversion in the full Laplace–Fourier domain

So far we have presented the sequentially ordered single-frequency inversion in the conventional frequency domain and Laplace–Fourier domain separately. Unlike the conventional waveform inversion algorithm performed as a two-step process, we will combine the Laplace-domain waveform inversion, the Laplace–Fourier domain waveform inversion and the conventional frequency-domain waveform inversion into a one-step process of waveform inversion in the full Laplace–Fourier domain. Although we have to choose from several sequential orders for waveform inversion shown in Fig. 3, we propose one sequential order of complex-valued frequencies for the sequential single-frequency waveform inversion in the full-Laplace domain inversion (Fig. 4). In this sequential order, we already include multiloop implementation of the conventional frequency-domain waveform inversion with small damping factors of 0.75, 0.5 and 0.15. Depending on the model complexity and the number of iterations per frequency, then, the inversion results might converge to the global minimum at just one loop or within a few loops. Please note that there might be other sequential orders for the waveform inversion that produce similar or better results. We will present the numerical examples of the sequentially ordered single-frequency inversion in the full Laplace–Fourier domain applied to the BP model and the field data.

SYNTHETIC EXAMPLES

SEG overthrust model (conventional frequency domain)

To examine the necessity and validity of the multiloop implementation of the sequentially ordered single-frequency waveform inversion, we conducted numerical experiments. Our test model was the SEG overthrust model (Aminzadeh *et al.* 1997) shown in Fig. 5. We simulated the observed data using a fourth order in space and second order in time finite-difference modelling code. The recording time was 16 s. The number of shots was 199 and the shotpoint interval was 100 m. The number of receivers was 801 and the receiver interval was 25 m. The grid interval of the model was 25 m. The initial model for the inversion was the homogeneous velocity model with a velocity of 4.0 km s^{-1}. We sequentially inverted 49 frequencies ranging from 0.25 to 12.25 Hz with a 0.25 Hz interval.

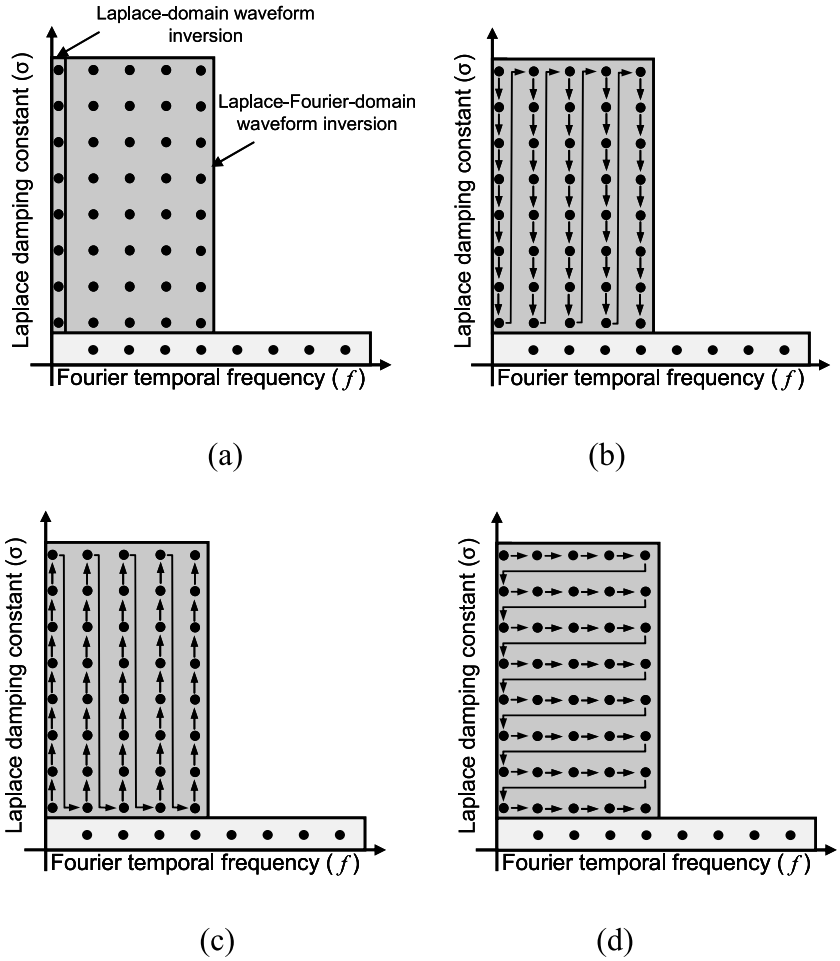

Figure 3. (a) Wavefield domains of the Laplace and Laplace–Fourier domain waveform inversion, (b–d) the three different sequential orders of the Laplace–Fourier domain waveform inversion: (b) the downward inversion path, (c) the upward inversion path and (d) the layer stripping inversion path.

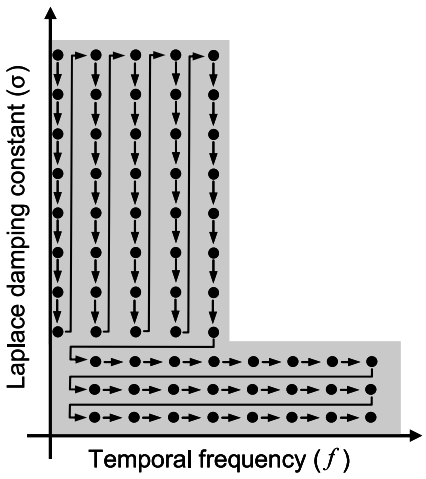

Figure 4. Wavefield domain and sequential orders of the sequentially ordered single-frequency waveform inversion in the full Laplace–Fourier domain.

The number of iterations was 25 for each frequency. At the first iteration for each frequency, the source wavelet was estimated, but the velocity was not updated. At the other 24 iterations, the velocity and the source wavelet were estimated and updated simultaneously. The step length was fixed as 25 m s^{-1} and the velocities were forced

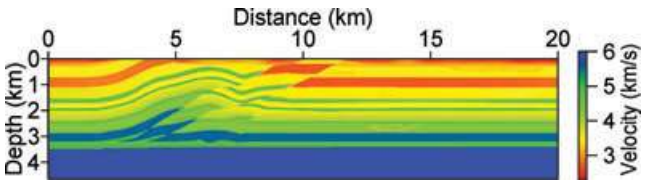

Figure 5. The true SEG overthrust velocity model.

to be between 2.3 and 6 km s^{-1}. Although the optimum step length may be found by appropriate analysis of the objective function, such as line-search techniques, we simply limited the maximum model update without the additional computation for choosing the step length. The inverted velocity models after 0.25, 2, 6 and 12.25 Hz are shown in Fig. 6. As the higher frequencies were inverted, the higher wavenumbers of the model were recovered. Note, however, that the high-velocity layer at the lower part of model, which was partially recovered at 2 and 6 Hz, was somewhat degraded at 12.25 Hz. This seems to be caused by individual matching at each frequency, and the best model at some frequencies may not be the best model at other frequencies. Therefore, the additional waveform inversion needs to be re-initiated from the first or lowest frequency using the final model at the highest frequency of the previous loop as a starting model.

Next, we will compare the inversion results with different numbers of iterations for each frequency and different outer loops, but

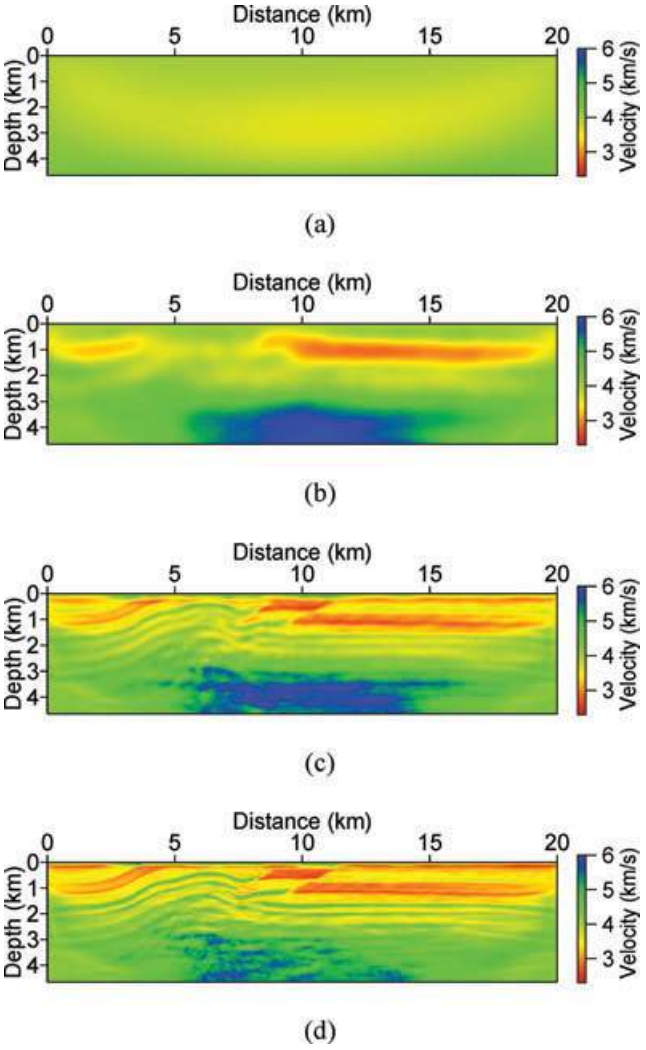

Figure 6. Inverted velocity models of the sequentially ordered single-frequency waveform inversion in the conventional frequency domain using a homogeneous velocity model of 4.0 km s^{-1}: (a) 0.25 Hz, (b) 2 Hz, (c) 6 Hz and (d) 12.25 Hz for the SEG overthrust synthetic data.

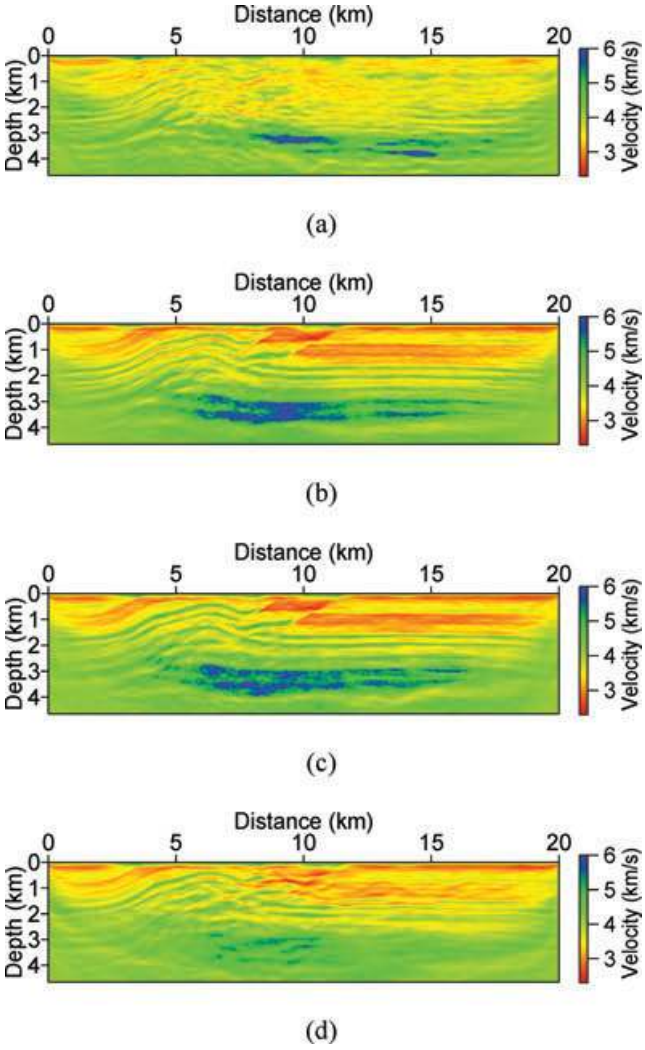

Figure 7. Comparison of the inverted velocity models of the conventional frequency-domain waveform inversion for the SEG overthrust synthetic data with different numbers of iterations for each frequency and different loops: (a) 1 and 12, (b) 3 and 4, (c) 6 and 2 and (d) 12 and 1. The number of total iterations of each frequency is equal to 12.

with the same number of iterations for entire frequencies. We performed four runs of the waveform inversion using 1, 3, 6 and 12 iterations per frequency, respectively (Fig. 7). The middle loop was over 49 frequencies. Figs 7(a)–(d) show the inversion results after 12 loops, 4 loops, 2 loops and 1 loop, respectively (Table 1). For example, 12 loops means repeating the middle loop 12 times. The number of total iterations per frequency is equal to 12 (number of iterations per frequency × number of loops, $n_{iter} \times n_{loop}$). The waveform inversion using one iteration per frequency produced the poorest results, even with the largest number of outer loops. However, the inversion results obtained using three and six iterations per frequency were better than that using 12 iterations and after only one loop, because the waveform inversions over entire frequencies were iteratively carried out several times. Fig. 8 shows the inversion results after 60, 20, 10 and 5 outer loops, using the same iterations per frequency (Table 1). The number of total iterations per frequency is equal to 60. The waveform inversion obtained using one iteration per frequency still produced the poorest results, even with the largest number of loops. Although the result obtained using 12 iterations per frequency looks slightly better, all of the other results seem to be acceptable. From these numerical experiments, we can conclude that the multiloop implementation improves the waveform inversion results, and the number of iterations per frequency is less important than the conventional double-loop implementation of the sequential waveform inversion. Moreover, because we can examine and compare the final results at the last frequency of each loop, we can perform additional quality control of the inversion results.

BP model (Laplace and Laplace–Fourier domain)

Now we present the simultaneous inversion and sequential inversion results in the Laplace and Laplace–Fourier domains following three sequential orders (Figs 3b–d). Our test model was the BP model (Billette & Brandsberg-Dahl 2005) shown in Fig. 9(a). We simulated the observed data using a fourth order in space and second order in time finite-difference modelling code. The recording time was 20 s and the sampling interval was 4 ms. The number of shots was 418 and the shotpoint interval was 200 m. The number of receivers was 301 and the receiver interval was 50 m. The acquisition geometry simulated the conventional marine acquisition towing the streamer. The length of the streamer was 15 km and the nearest

Table 1. Summary of the number of iterations per frequency, the number of frequencies and the number of loops for Figs 7 and 8.

Figure number	Frequencies (f) and number of frequencies (n_f)	Number of iterations at a single-frequency loop (n_{iter})	Number of loops (n_{loop})	Number of total iterations per frequency ($n_{iter} \times n_{loop}$)
Fig. 7(a)		1	12	12
Fig. 7(b)	0.25–12.25 Hz, 0.25 Hz	3	4	
Fig. 7(c)	interval, 49 frequencies	6	2	
Fig. 7(d)		12	1	
Fig. 8(a)		1	60	60
Fig. 8(b)	0.25–12.25 Hz, 0.25 Hz	3	20	
Fig. 8(c)	interval, 49 frequencies	6	10	
Fig. 8(d)		12	5	

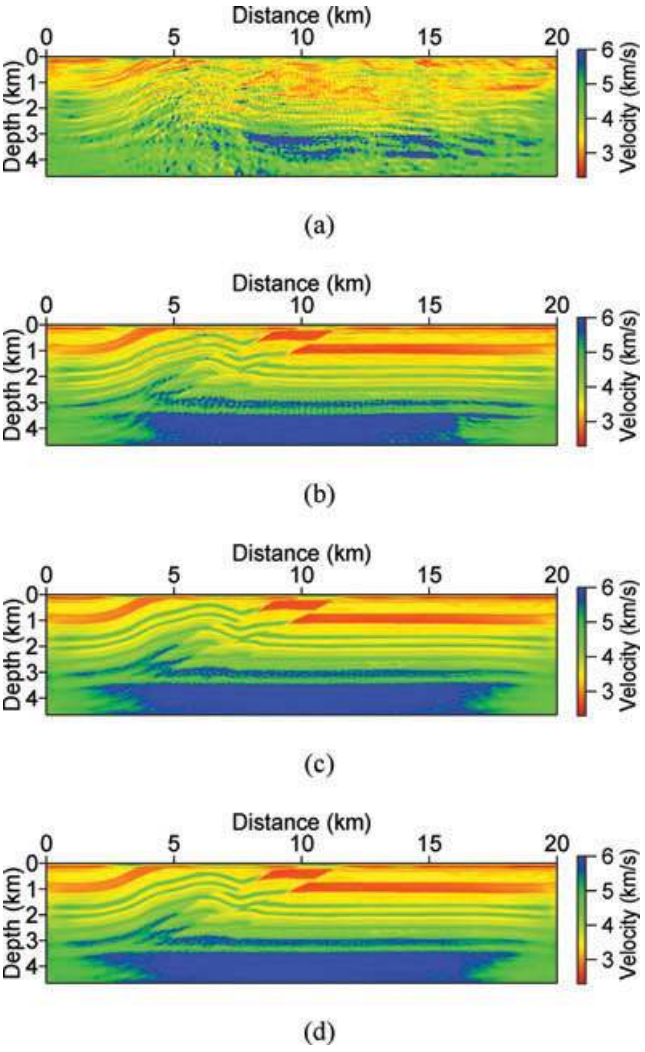

Figure 8. Comparison of the inverted velocity models of the conventional frequency-domain waveform inversion for the SEG overthrust synthetic data with different numbers of iterations for each frequency and different loops: (a) 1 and 60, (b) 3 and 20, (c) 6 and 10 and (d) 12 and 5. The number of total iterations of each frequency is equal to 60.

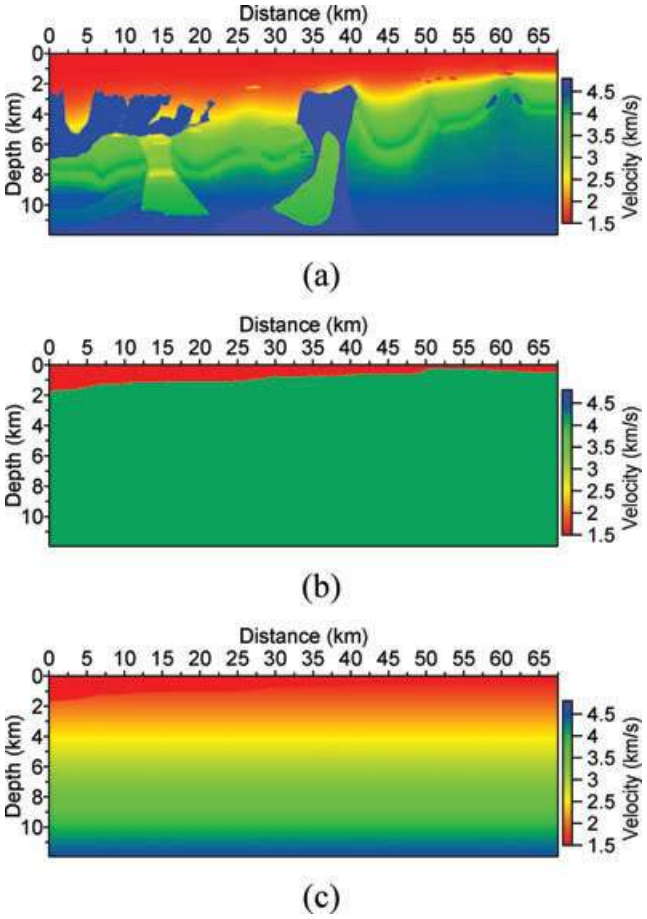

Figure 9. (a) The true BP velocity model, (b) the two-layer homogenous initial velocity model with a velocity of 4.1 km s^{-1} and (c) the linearly increasing velocity model varying from 1.5 to 4.5 km s^{-1}.

offset was 0. The first derivative of the Gaussian function was used for the source wavelet. The two-layer homogeneous velocity model, with a velocity of 4.1 km s^{-1} (Fig. 9b), and the linearly increasing velocity model, varying from 1.5 to 4.5 km s^{-1} (Fig. 9c), were used as starting models. The velocity of the sea water layer was fixed at 1.5 km s^{-1}. The grid interval of the model for inversion was 50 m. Seven Laplace damping constants ranging from 1 to 13 with an interval of 2, and seven frequencies ranging from 0.01 to 1.51 Hz with an interval of 0.25 Hz, were used. Therefore, a total of 49 complex-valued damping constants were used. The number of iterations for each frequency was seven. At the first iteration of each frequency, the source wavelet was estimated, but the velocity was not updated. The step length was fixed at 50 m s^{-1} and the velocities were forced to be between 1.3 and 4.8 km s^{-1}.

The inversion result using the Laplace-domain simultaneous waveform inversion at the 210th iteration is shown in Fig. 10(a).

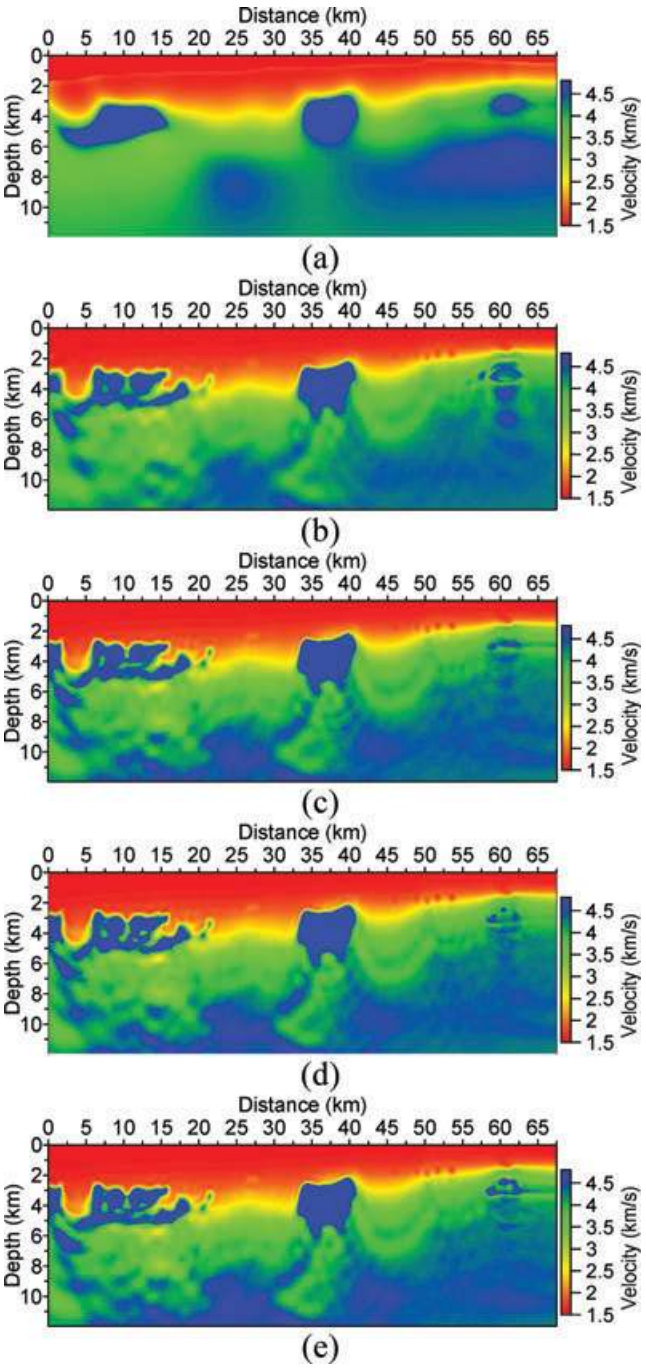

Figure 10. Inverted velocity models of the simultaneous (a and b) and sequential (c–e) inversion in the Laplace–Fourier domain for the BP synthetic data: (a) Laplace domain simultaneous inversion; (b) Laplace–Fourier domain simultaneous inversion from (a); (c–e) downward path, upward path and layer stripping path of the sequentially ordered single-frequency inversion in the Laplace–Fourier domain, respectively.

We performed a waveform inversion on a Linux PC cluster, with each node comprising two quad-core Intel Xeon 2.5 GHz processors; each node had eight cores. In our MPI (message passing interface) environment, each core of the eight-core nodes was assigned a single MPI process. At each iteration, each CPU core inverted a single Laplace damping constant, and a total of seven cores were used for seven Laplace damping constants, ranging from 1 to 13 with an interval of 2. The Fourier temporal frequency was 0.01 Hz. The total computation time for completing 210 iterations was 369 min. A smooth background velocity model, including a linearly increasing velocity trend and high-velocity salt domes, was recovered well from the two-layer homogeneous velocity model (Fig. 9b). Using this result as a starting model, we performed the simultaneous waveform inversion in the Laplace–Fourier domain. From the inversion results at the 500th iteration, shown in Fig. 10(b), it is evident that the medium-wavelength velocity model was recovered well. A total of 42 CPU cores were used for 42 complex-valued damping constants (seven Laplace damping constants ranging from 1 to 13 with an interval of 2, and six frequencies ranging from 0.26 to 1.51 Hz with an interval of 0.25 Hz). The total core time for completing 500 iterations was 907 min.

The inversion results from the sequentially ordered single-frequency inversion in the Laplace–Fourier domain following the three sequential orders after the 10th loop are shown in Figs 10(c)–(e). Note that the inversion results are almost similar. A total of nine CPU cores were used. At each iteration, the multiple shots were grouped into nine groups, and a single CPU core inverted each group of shots. The total computation time for completing 10 loops was 1100 min. In our experiments, we used the full size of the domain for every group of shots and all CPU cores calculated the same LU factorization. However, if we used different subdomains with smaller sizes for each group of shots, the computation time would be reduced significantly.

From these numerical experiments, we can conclude that the sequentially ordered single-frequency inversion in the Laplace–Fourier domain can produce similar results to the simultaneous waveform inversion, but that less computational resources are required. As the number of frequencies used for waveform inversion in the Laplace–Fourier domain is increased, the computation efficiency is also increased. Because the multiloop implementation is adopted, the number of iterations per frequency is less important, and we can easily perform quality control of the inversion results.

BP model (one-step waveform inversion in the full Laplace–Fourier domain)

To validate the proposed one-step waveform inversion algorithm in the full Laplace–Fourier domain, we applied it to a synthetic data set generated from the BP model. The main targets of the model were a complex rugose multivalued salty body, the subsalt slow-velocity anomalies in the left part of the model, a deeply rooted salt body in the central part and the extra-salt and localized shallow anomalies in the right part (Billette & Brandsberg-Dahl 2005). The details of the synthetic data set are described in the previous section.

First, we performed the sequentially ordered single-frequency waveform inversion in the conventional frequency domain. Twenty-four frequencies ranging from 0.25 to 6.00 Hz, with a 0.25 Hz interval, were used. The number of iterations for each frequency was seven. At the first iteration for each frequency, the source wavelet was estimated, but the velocity was not updated. The step length was fixed as 50 m s^{-1} and the velocities were forced to be between 1.3 and 4.8 km s^{-1}. The final inversion result, using the linearly increasing velocity model (Fig. 9c) as a starting model at the 10th iteration, is shown in Fig. 11(a). Although the salt body in the left part, the top area of the salt body in the central part and some shallow anomalies were partially recovered, the overall inversion result was unsatisfactory.

Next, we performed the sequentially ordered single-frequency waveform inversion in the full Laplace–Fourier domain. A total

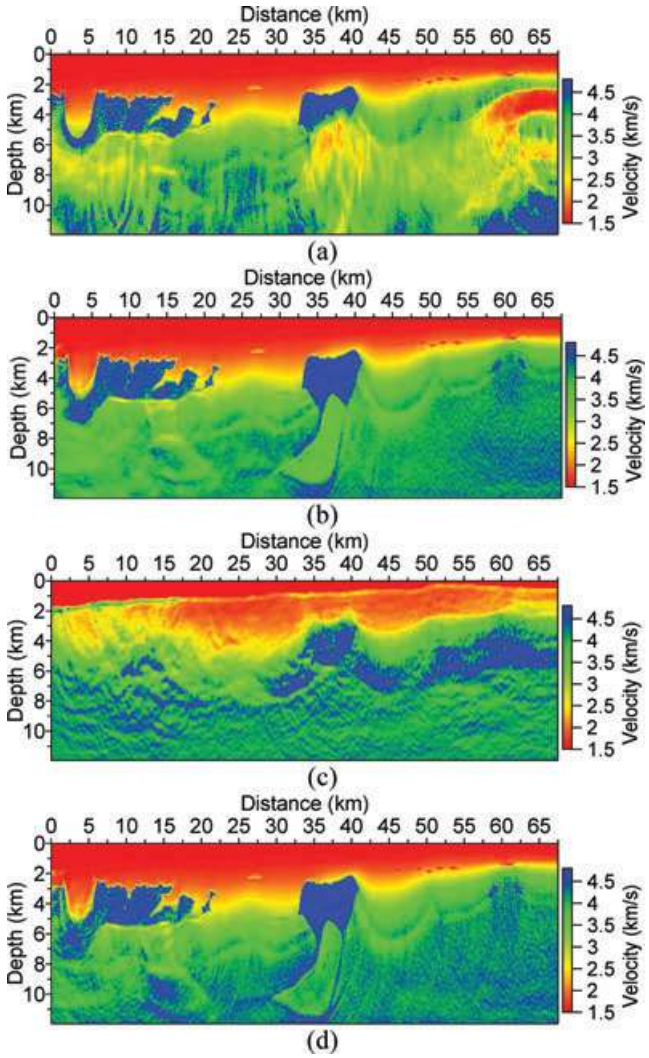

Figure 11. Inverted velocity models for the BP synthetic data using the sequentially ordered single-frequency inversion (a) in the conventional frequency domain using the linearly increasing velocity model after the 10th loop and (b–d) in the Laplace–Fourier domain using the two-layer homogeneous velocity model after (b) the first loop, (c) the first loop and (d) the fourth loop, respectively. The number of iterations for each frequency is (a and b) 6 and (c and d) 2.

of 247 complex-valued frequencies were used for the inversion: (1) seven damping constants ranging from 1 to 13 with an interval of 2 and 25 frequencies ranging from 0.01 to 6.01 Hz with a 0.25 Hz interval ($7 \times 25 = 175$ complex-valued frequencies) and (2) 24 frequencies ranging from 0.25 to 6.00 Hz with a 0.25 Hz interval with three small damping factors of 0.75, 0.5 and 0.15 ($3 \times 24 = 72$ complex-valued frequencies). The sequential order of complex-valued frequencies for the inversion is shown in Fig. 4. The initial velocity model is the two-layer homogeneous velocity model shown in Fig. 9(b). The inversion result obtained using six iterations for velocity update per frequency after the first loop is shown in Fig. 11(b). Several salt bodies, subsalt low-velocity anomalies and localized shallow anomalies were well recovered even after the first loop and when using the two-layer homogeneous velocity model as a starting model.

To understand the behaviour of the proposed algorithm using different iterations per frequency, we performed another run of the proposed waveform inversion using two iterations for velocity update per frequency. The inverted velocity models after the first and fourth loop are shown in Figs 11(c) and (d), respectively. Fig. 11(c) obviously indicates that the recovery of the velocity structures after the first loop was incomplete, which might have been caused by the insufficient number of iterations per frequency. However, we can observe that the velocity structures were improved considerably after the fourth loop, although some artefacts appeared around the salt body in the right part (Fig. 11d).

These numerical experiments demonstrate that the number of iterations per frequency in our algorithm is less important than in the conventional double-loop algorithm. The successful recovery of the target features even when using the two-layer homogeneous velocity model shows the robustness of our algorithm.

REAL DATA CASE STUDIES

Field data set (the Gulf of Mexico)

In this section, we apply our algorithm to real data to examine the field applicability. The field data are the data set acquired from the Gulf of Mexico. The number of shots was 399 and the shot-point interval was 50 m. The number of channels was 408 and the receiver interval was 25 m. The recording length was 12 s and the sampling interval was 4 ms. The offset range was 137 m to 10.321 km. The water depth ranged from 420 to 910 m. An example of the raw shot gather is shown in Fig. 12(a). First arrivals, such as direct wave and refractions wave, are clearly seen. Although we do not show the frequency spectrum here, the frequency band below 4 Hz seemed to be unreliable. A damped shot gather with a damping constant of 1.0 is shown in Fig. 12(b). Late arrivals were almost damped and early arrivals such as direct wave, refraction wave and shallow reflections were dominant. Fig. 12(c) shows the amplitude spectra of the Laplace–Fourier transformed wavefield of 0.01 Hz with different damping constants. At a very small damping constant ($\sigma = 0.01$), the amplitude spectra were highly variable with the offset. At the Laplace damping constant of 1, the amplitude spectra were still highly variable with offset, even though most of the late arrivals are damped. However, as we can see in the synthetic example shown in Fig. 1, the tendency of the amplitude spectra to decrease exponentially with offset is apparent when the Laplace damping constant is larger. Considering the small amplitude values of the Laplace-transformed wavefields, we can understand that the logarithmic waveform inversion is suitable for the Laplace domain waveform inversion (Shin & Cha 2008, 2009).

First, we applied a sequentially ordered single-frequency inversion in the conventional frequency domain. The starting model was the linearly increasing velocity model varying from 1.5 to 2.85 km s^{-1}, but the velocity of the sea water layer was fixed as 1.5 km s^{-1}. The grid interval for inversion was 18 m. Sixty frequencies were used, ranging from 0.25 to 15.00 Hz with a 0.25 Hz interval. The number of iterations for each frequency was seven. At the first iteration of each frequency, the source wavelet was estimated, but the velocity was not updated. The step length was fixed as 25 m s^{-1} and the velocities were forced to be between 1.3 and 4.8 km s^{-1}. The final inversion result at the eighth loop is shown in Fig. 14(a). The velocity of the shallow sedimentary structures was recovered to some extent, but the velocity of the salt structure in the central part was not recovered at all.

Next, we carried out the sequentially ordered single-frequency waveform inversion in the full Laplace–Fourier domain. The starting model was a two-layer velocity model in which the first layer was

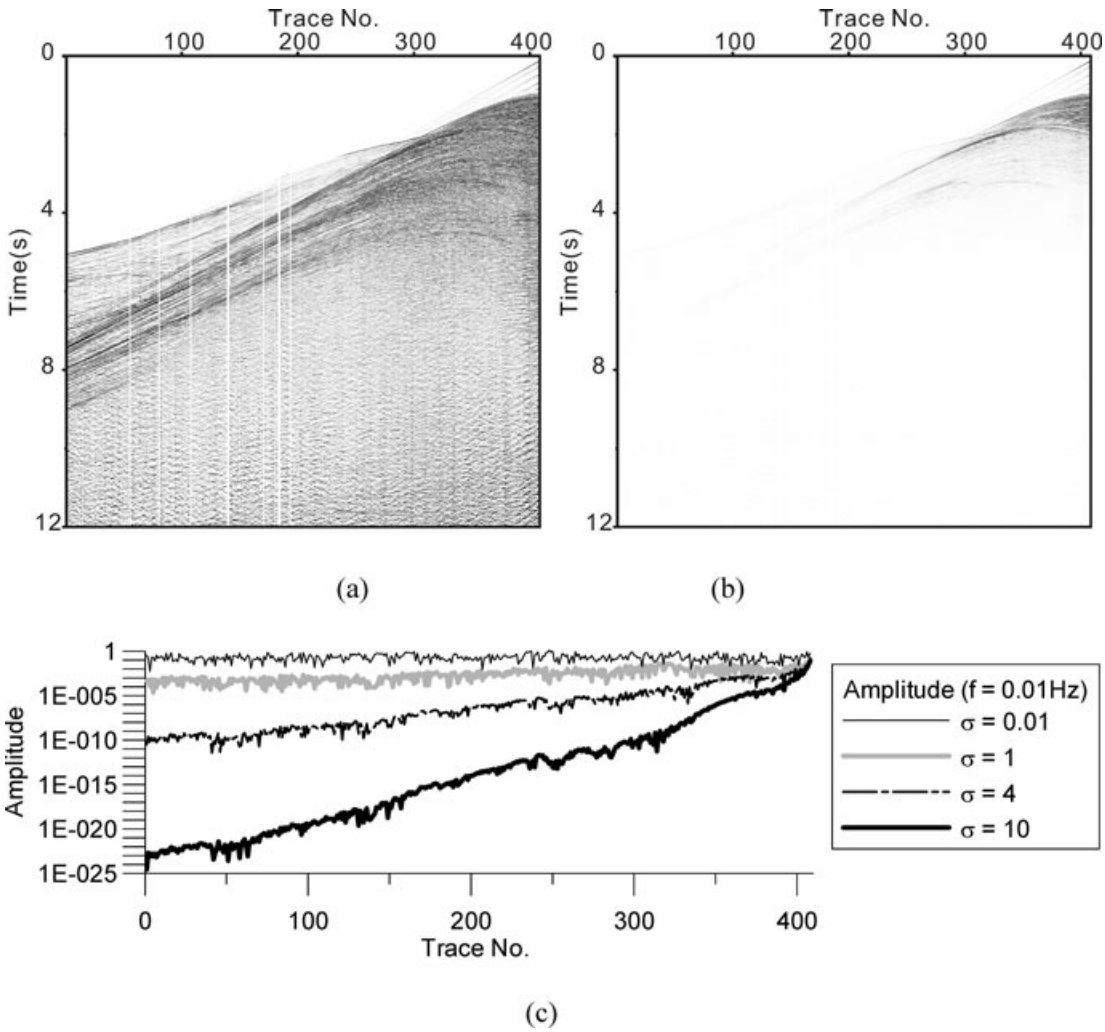

Figure 12. Real data example (Gulf of Mexico): an example of (a) raw shot gather acquired in the Gulf of Mexico and (b) damped shot gather with a damping constant of 1.0. (c) shows the amplitude spectra of the Laplace–Fourier transformed wavefields with different Laplace damping constants at 0.01 Hz.

the sea water and the second layer was the homogeneous model with a velocity of 3.3 km s^{-1}. A total of 237 complex-valued frequencies were used for the inversion: (1) 6 damping constants ranging from 2 to 12 with an interval of 2 and 17 frequencies ranging from 0.01 to 4.01 Hz with a 0.25 Hz interval ($6 \times 17 = 102$ complex-valued frequencies) and (2) 45 frequencies ranging from 4.00 to 15.00 Hz with a 0.25 Hz interval and with three small damping factors of 0.75, 0.5 and 0.15 ($3 \times 45 = 135$ complex-valued frequencies). A strategy choosing complex-valued frequencies and sequential orders for inversion is shown in Figs 4 and 13. We first performed the sequential inversion in the Laplace domain using six damping factors and 0.01 Hz, three times, to get a more reasonable background model. We then performed the sequential inversion using the above 237 complex-valued frequencies (Fig. 13). The number of iterations needed for the velocity update for each frequency was six, except for the first iteration for the source wavelet estimation.

The intermediate velocity model from the Laplace-domain waveform inversion (six damping constants, six iterations, three outer loops) is shown Fig. 14(b). The long-wavelength velocity model was recovered from the two-lay homogeneous velocity model. The final result after the first loop is shown in Fig. 14(c). The high velocity of the main salt body in the central part was clearly recovered. This was impossible in the conventional frequency-domain waveform inversion. To assess the reliability of the inverted velocity model, we performed the pre-stack reverse-time depth migration in the frequency domain. Fig. 15(a) shows the migrated image from the pre-stack reverse-time depth migration using the two-layer initial velocity model, whereas Fig. 15(b) shows the corresponding migrated image using the inverted velocity structure. The salt boundaries, shallow-layered sedimentary structures and faults are imaged clearly. We compared the common-image gathers from the reverse-time migration using the initial velocity model and the inverted velocity structure at a distance of 4.14 and 14.58 km (Fig. 16). Figs 16(a) and (b) show the common-image gathers using the initial velocity structure, whereas Figs 16(c) and (d) show the common-image gathers using the inverted velocity model. Judging from the fact that most reflection events in the common-image gathers using the inverted velocity structure are flattened, the inverted velocity structure seems to be reasonable. These results demonstrate that the proposed waveform inversion technique can be applied to field data suffering from a lack of meaningful low-frequency information.

Field data set (Korean continental shelf)

We applied our algorithm to real data acquired from the offshore Korea. The number of shots was 522 and the shotpoint interval was

```
do loop = 1, n_loop
  do freq = 0.01                    (1 frequency)
    do sigma =12, 2, -2             (6 damping constants, n_f =6)
      do iter =1,7                  (7 iterations, n_iter =7)
        single-frequency waveform inverse
            in the Laplace domain
      enddo
    enddo
  enddo
enddo                               ⇨ Fig. 14b (nloop = 3)
do loop = 1, n_loop
  do freq = 0.01, 4.01, 0.25        (17 frequencies)
    do sigma =12, 2, -2             (6 damping constants, n_f = 6x17= 102)
      do iter =1,7                  (7 iterations, n_iter =7)
        single-frequency waveform inverse
            in the Laplace-Fourier frequency domain
      enddo
    enddo
  enddo
  do sigma[] = { 0.75, 0.5, 0.15}   (3 damping constants)
    do freq = 4.00,15.00,0.25       (45 frequencies, n_f = 3x45 = 135)
      do iter =1,7                  (7 iterations, n_iter =7)
        single-frequency waveform inverse
            in the frequency domain
      enddo
    enddo
  enddo
enddo                               ⇨ Fig. 14c (nloop = 1)
```

Figure 13. A strategy choosing complex-valued frequencies and sequential orders for a sequentially ordered single-frequency waveform inversion in the Laplace–Fourier domain for the field data set from the Gulf of Mexico.

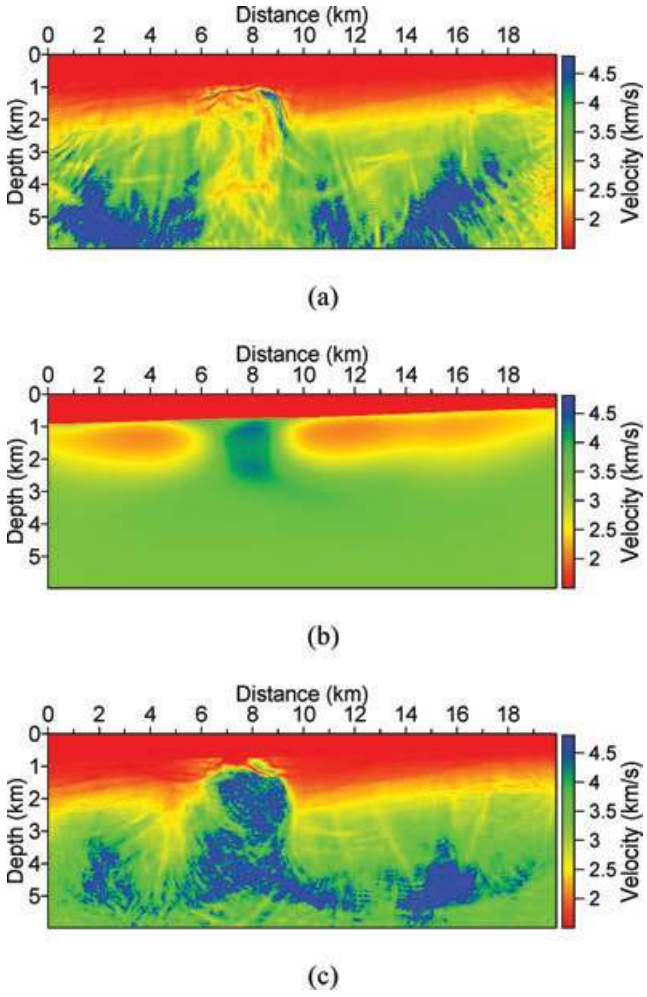

Figure 14. Real data example (Gulf of Mexico): inverted velocity models from the sequentially ordered single-frequency inversion (a) in the conventional frequency domain using the linearly increasing velocity model after the eighth loop, (b) in the Laplace domain using the two-layer homogeneous velocity model after the third loop and (c) in the Laplace–Fourier domain using the two-layer homogeneous velocity model after the first loop, respectively.

50 m. The number of channels was 160 and the receiver interval was 12.5 m. The offset ranged from 150 m to 2.1375 km. The recording length was 9 s and the sampling interval was 2 ms. Fig. 17(a) shows the near trace gather after low-pass filtering up to 50 Hz and gain correction. We can see the strong multiples and the shallow sedimentary layers, including faults and folding structures. Although the recording time was sufficiently long, the streamer length was too short to obtain the deep velocity model from the Laplace and Laplace–Fourier domain waveform inversion. We aimed to evaluate our algorithm by trying to invert the short-offset field data using the simple velocity model. The initial model was a two-layer velocity model, in which the first layer was the sea water and the second layer was the homogeneous model with a velocity of 2.5 km s^{-1}. We confined the maximum recovering depth to 1.25 km. The grid interval for the waveform inversion was 12.5 m. The number of iterations needed for the velocity update for each frequency was three. The step length was fixed as 10 m s^{-1} and the velocities were forced to be between 1.3 and 3.3 km s^{-1}.

The strategy for choosing the sequential order of complex-valued frequencies for inversion was similar to that shown in Fig. 13, but the composition of the complex-valued frequencies was different. A total of 327 complex-valued frequencies were used for the inversion: (1) 7 damping constants ranging from 3 to 21 with an interval of 3 and 12 temporal frequencies ranging from 0.01 to 2.76 Hz with a 0.25 Hz interval ($7 \times 12 = 84$ complex-valued frequencies) and (2) 81 frequencies ranging from 5.25 to 25.25 Hz with a 0.25 Hz interval with three small damping factors of 0.75, 0.5 and 0.15 ($3 \times 81 = 243$ complex-valued frequencies). The final inverted velocity model from the waveform inversion is shown in Fig. 17(b). The large-scale velocity structures, the small-wavelength features and the relatively high-velocity zone between horizontal distances 0 and 8 km were recovered well from the two-layer initial velocity model. To assess the validity of the inverted velocity model, we compared the real seismogram, band-pass filtered from 5.25 to 25.25 Hz, with the synthetic seismogram generated from the inverted velocity model when the source was located at 22.8125 km (Fig. 18). The real data seemed comparable to the synthetic seismogram from the final velocity model but some discrepancies could be found. The possible causes of the inconsistency may have been the 2-D, constant-density, acoustic approximation to 3-D heterogeneous earth, the short-offset data or the low signal-to-noise ratio. We compared the migrated images from the Kirchhoff pre-stack depth migration using the two-layer initial velocity model and the inverted velocity structure (Fig. 19). The shallow reflectors are unclear on the migrated image from the initial velocity model shown in Fig. 19(a), whereas the reflectors are well focused on the migrated images from the inverted velocity model shown in Fig. 19(b), and the overall quality of the migrated image appears to be much improved. This second real

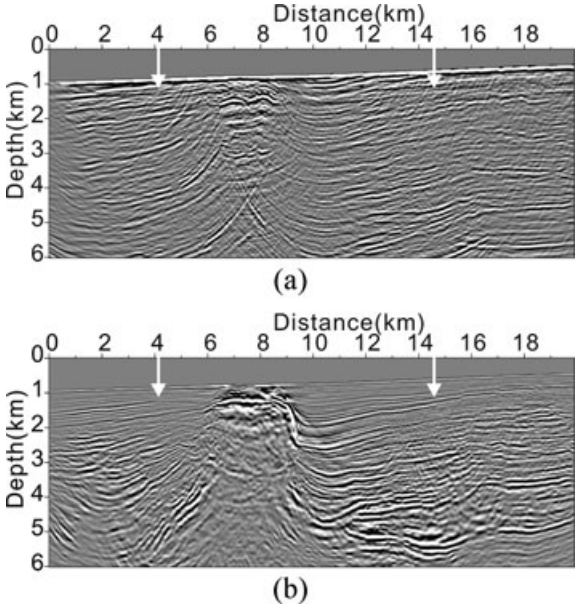

Figure 15. Reverse-time migrated images from (a) the initial velocity model and (b) the inverted velocity structure for the field data set from the Gulf of Mexico.

data example shows the field applicability and performance of the proposed algorithm.

CONCLUSIONS

We have presented a sequentially ordered 2-D acoustic waveform inversion algorithm in the full Laplace–Fourier domain. This algorithm has combined all Laplace, Laplace–Fourier and conventional frequency domain waveform inversions into a one-step process. Our algorithm has the advantages of both the sequential inversion technique and the Laplace–Fourier domain waveform inversion algorithm, including computational efficiency, stability, robustness and low dependence on the initial model. Our algorithm also seeks to find a final velocity structure from simple starting models, such as the two-layer homogeneous velocity model or the linearly increasing velocity model.

The sequentially ordered single-frequency waveform inversion in the conventional frequency domain has been implemented mostly as a double-loop algorithm. However, it was difficult to determine how many iterations we needed to perform at each frequency and to assign a proper stopping criteria. To overcome these difficulties, we adopted a multiloop implementation for the sequentially ordered single-frequency logarithmic waveform inversion, where the additional waveform inversion is iteratively re-initiated from the first or lowest frequency using the final model at the highest frequency of the previous loop as a starting model. From the numerical experiments using the SEG overthrust model, we have shown that the multiloop implementation improved the waveform inversion results, and that the number of iterations per frequency was less important than the conventional double-loop implementation of the sequential waveform inversion.

The multiloop implementation of the sequentially ordered single-frequency inversion was applied to the sequentially ordered single-frequency inversion in the Laplace and Laplace–Fourier domain waveform inversions. The main differences were the composition of the frequencies used, the corresponding wavefields and the sequential order. Because the Laplace–Fourier wavefield domain is a 2-D plane, we had to assign a sequential order of complex-valued frequencies in a 2-D plane for sequential inversion. Thus, we have presented three sequential orders that consider the conventional multiscale inversion approach and the layer-stripping approach. From the numerical experiments using the BP model, three types of sequentially ordered single-frequency inversions in the Laplace–Fourier domain produced similar results to the simultaneous waveform inversion, but less computational resources were required.

Based on these numerical experiments, we combined the Laplace-domain waveform inversion, the Laplace–Fourier waveform inversion and the conventional frequency-domain waveform inversion into a one-step process of waveform inversion in the full Laplace–Fourier domain. Our one-step waveform inversion, the sequentially ordered single-frequency 2-D acoustic waveform inversion in the full Laplace–Fourier domain, was applied to the synthetic data set from the BP model and field data. Although the inversion results from the conventional frequency-domain inversion using the linearly increasing velocity model as a starting model were insufficient, our algorithm recovered reasonably complex velocity structures, even using the two-layer homogeneous velocity model as a starting model. The inversion results derived from the field data were validated by examining the migrated image from the pre-stack depth migration and the flattening of the common-image gathers,

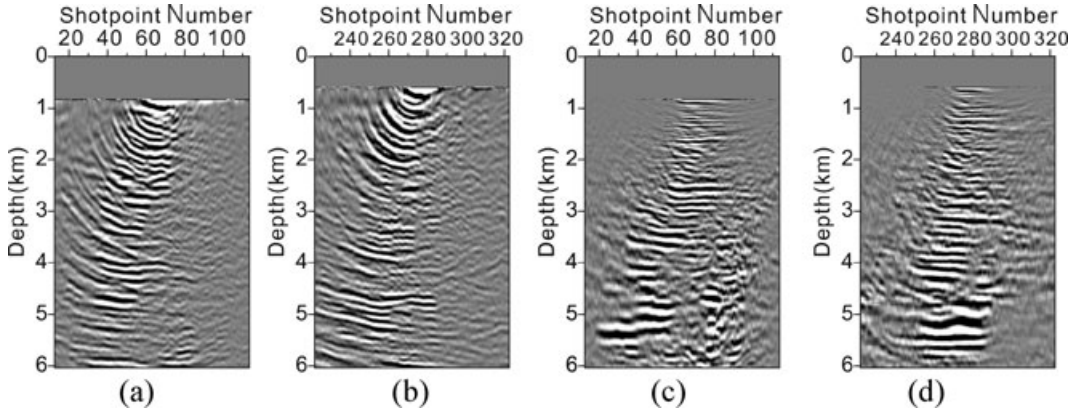

Figure 16. Comparison of the common-image gathers from the pre-stack reverse-time migration using (a and b) the initial velocity model and (c and d) the inverted velocity structure; (a) and (c) are the common-image gathers at a distance of 4.14 km and (b) and (d) are the common-image gathers at a distance of 14.58 km, respectively.

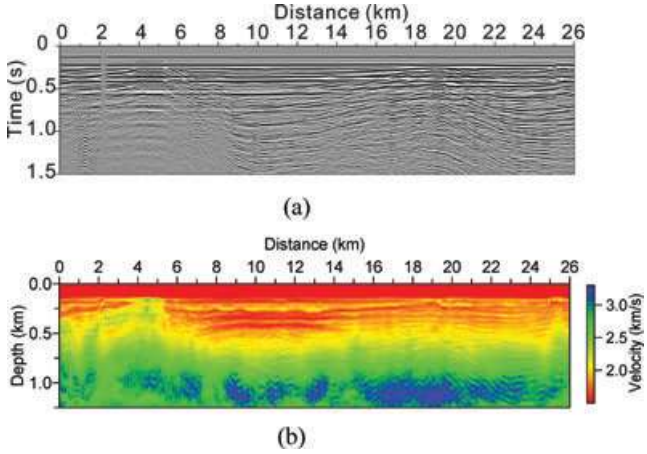

Figure 17. Real data example (Korean continental shelf): (a) the near trace gather, and (b) the inverted velocity model from the sequentially ordered single-frequency inversion in the Laplace–Fourier domain using the two-layer homogeneous velocity model.

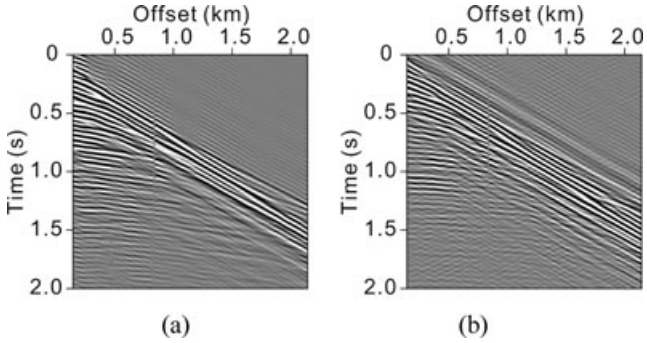

Figure 18. Comparison of (a) field seismogram with (b) synthetic seismogram generated from the inverted velocity structure when the source is located at 22.8125 km.

or they were validated by comparing the synthetic shot gather with the real shot gather.

However, it is important to recognize that the inverted velocity model from the field data could still represent a local minimum that might be caused by the limitations of the acoustic approximation to wave propagation through the real earth, the constant-density approximation, the 2-D approximation to a 3-D wavefield or the low signal-to-noise ratio. Therefore, the extension of our sequential inversion algorithm to 2-D acoustic joint inversion for velocity and density, 2-D elastic waveform inversion and 3-D acoustic- and elastic-waveform inversion should be studied. Moreover, the optimum selection of the complex-valued damping constants still needs to be investigated.

ACKNOWLEDGMENTS

This work was financially supported by the Brain Korea 21 Project of the Ministry of Education, Science and Technology. N.-H. Koo and K.-P. Park were supported by the Ministry of Knowledge Economy funding to the Korea Institute of Geoscience and Mineral Resources. The authors thank GX Technology for providing the data set of the Gulf of Mexico, and we are grateful to BP and Frederic Billette for providing the BP velocity model and data.

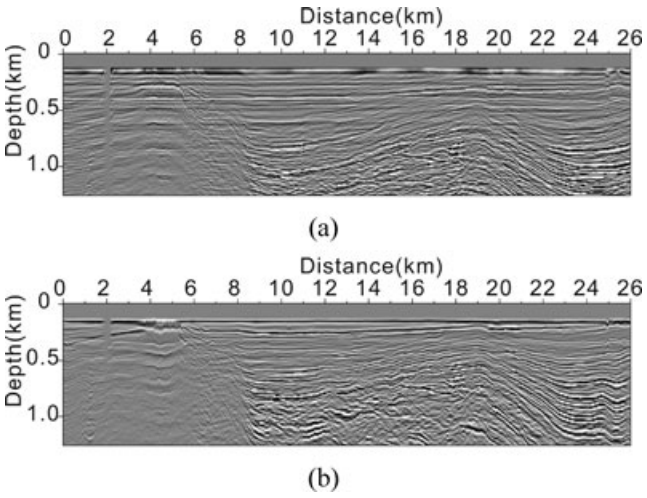

Figure 19. Comparison of the pre-stack Kirchhoff depth-migrated images using (a) the two-layer initial velocity model and (b) the inverted velocity structure for the field data set from the Korean continental shelf.

REFERENCES

Aminzadeh, F., Brac, J. & Kunz, T., 1997. *3-D Salt and Overthrust Models,* SEG/EAGE 3-D Modeling Series 1, SEG.

Ben-Hadj-Ali, H., Operto, S. & Virieux, J., 2008. Velocity modeling building by 3D frequency-domain, full-waveform inversion of wide-aperture seismic data, *Geophysics,* **73,** VE101–VE117.

Billette, F.J. & Brandsberg-Dahl, S., 2005. The 2004 BP Velocity Benchmark, in *Proceedings of the 67th Meeting, Madrid, Spain, June 13–16, 2005, EAGE, Extended Abstracts,* B035.

Bleibinhaus, F., Lester, R.W. & Hole J.A., 2008. Applying waveform inversion to wide-angle seismic surveys, *Tectonophysics,* doi: 10.1016/j.tecto.2008.08.023.

Brenders, A.J. & Pratt, R.G., 2007. Full waveform tomography for lithospheric imaging: results from a blind test in a realistic crustal model, *Geophys. J. Int.,* **168,** 133–151.

Bunks, C., Saleck, F.M., Zalesk, S. & Chavent, G., 1995. Multiscale seismic waveform inversion, *Geophysics,* **60,** 1457–1473.

Hu, W., Abubakar, A. & Habashy, T., 2007. Simultaneous frequency-domain seismic full-waveform data inversion, in *Proceedings of the 69th Meeting, London, UK, June 11–14, 2007, EAGE, Extended Abstracts,* C028.

Jaiswal, P., Zelt, C.A., Bally, A.W. & Dasgupta, R., 2008. 2-D traveltime and waveform inversion for improved seismic imaging: Naga Thrust and Fold Belt, India, *Geophys. J. Int.,* **173,** 642–658.

Jang, U., Min, D.-J. & Shin, C., 2009. Comparison of scaling methods for waveform inversion, *Geophys. Prospect.,* **57,** 49–59.

Lailly, P., 1983. The seismic inverse problems as a sequence of before stack migrations, in *Conference on Inverse Scattering: Theory and Applications,* pp. 206–220, eds Bednar, J.B., Redner, R., Robinson, E. & Weglein, A., Society for Industrial and Applied Mathematics, Philadelphia.

Lee, L.H. & Kim, H.J., 2003. Source-independent full-waveform inversion of seismic data, *Geophysics,* **68,** 2010–2015.

Marfurt, K., 1984. Accuracy of finite-difference and finite-elements modelling of the scalar and elastic wave equation, *Geophysics,* **49,** 533–549.

Mora, P., 1987. Nonlinear two-dimensional elastic inversion of multioffset seismic data, *Geophysics,* **52,** 1211–1228.

Operto, S., Virieux, J., Dessa, J.-X. & Pascal, G., 2006. Crustal seismic imaging from multifold ocean bottom seismometer data by frequency domain full waveform tomography: application to the eastern Nankai trough, *J. geophys. Res.,* **111,** B09306.

Pratt, R.G., 1999. Seismic waveform inversion in the frequency domain. Part 1: Theory and verification in a physical scale model, *Geophysics,* **64,** 888–901.

Pratt, R.G., Shin, C. & Hicks, G.J., 1998. Gauss-Newton and full Newton methods in frequency-space seismic waveform inversion, *Geophys. J. Int.,* **133,** 341–362.

Pratt, R.G. & Worthington, M.H., 1990. Inverse theory applied to multi-source cross-hole tomography. Part 1: Acoustic wave-equation method, *Geophys. Prospect.,* **38,** 287–310.

Sheen, D.-H., Tuncay, K., Baag, C.-E. & Ortoleva, P.J., 2006. Time domain Gauss-Newton seismic waveform inversion in elastic media, *Geophys. J. Int.,* **167,** 1373–1384.

Shin, C. & Cha, Y.H., 2008. Waveform inversion in the Laplace domain, *Geophys. J. Int.,* **173,** 922–931.

Shin, C. & Cha, Y.H., 2009. Waveform inversion in the Laplace-Fourier domain, *Geophys. J. Int.,* **177,** 1067–1079.

Shin, C. & Ha, W., 2008. A comparison between behavior of objective functions for waveform inversion in the frequency and Laplace domains, *Geophysics,* **73,** VE119–VE133.

Shin, C., Jang S.H. & Min, D.-J., 2001. Improved amplitude preservation for prestack depth migration by inverse scattering theory, *Geophys. Prospect.,* **49,** 592–606.

Shin, C. & Min, D.-J., 2006. Waveform inversion using a logarithmic wavefield, *Geophysics,* **71,** R31–R42.

Shin, C., Pyun, S. & Bednar, J.B., 2007. Comparison of waveform inversion. Part 1: Conventional wavefield vs logarithmic wavefield, *Geophys. Prospect.,* **55,** 449–464.

Shipp, R.M. & Singh, S.C., 2002. Two-dimensional full wavefield inversion of wide-aperture marine seismic streamer data, *Geophys. J. Int.,* **151,** 325–344.

Sirgue, L. & Pratt R.G., 2004. Efficient waveform inversion and imaging: a strategy for selecting temporal frequencies, *Geophysics,* **69,** 231–248.

Tarantola, A., 1984. Inversion of seismic reflection data in the acoustic approximation, *Geophysics,* **49,** 1259–1266.

Tarantola, A., 1986. A strategy for nonlinear elastic inversion of seismic reflection data, *Geophysics,* **51,** 1893–1903.

Wu, R.S. & Toksöz, M.N., 1987. Diffraction tomography and multisource holography applied to seismic imaging, *Geophysics,* **52,** 11–25.

Yokota, T. & Matsushima, J., 2004. Seismic waveform tomography in the frequency-space domain: selection of the optimal temporal frequency for inversion, *Explor. Geophys.,* **35,** 19–24.